Fluidized-Bed and Fixed-Bed Reactor Testing of Methane Chemical Looping Combustion with MgO-Promoted Hematite

Duane D. Miller,[A,B,+] *Ranjani Siriwardane,*[A] *and James Poston,*[A]

[A]U.S. Department of Energy, National Energy Technology Laboratory, 3610 Collins Ferry Road, P.O. Box 880, Morgantown, WV 26507-0880

[B]URS Corporation, 3610 Collins Ferry Road, Morgantown, WV 26507-0880

[+]AUTHOR INFORMATION: Tel.: + 01- 304-285-5292. Fax: + 01-304-285-4403, E-mail: duane.miller@netl.doe.gov

ABSTRACT: In this study MgO-promoted Fe_2O_3 hematite oxygen carriers were synthesized from various Mg sources and evaluated for methane chemical looping combustion. Particles suitable for fluidized bed flow reactor studies were prepared in the lab. Cyclic CLC tests conducted in the fluidized bed with MgO promoted hematite showed better performance than that with hematite. Attrition resistance of laboratory prepared MgO promoted hematite was excellent. Reactivity and stability of the oxygen carrier materials were also tested in the thermogravimetric analyzer and bench-scale reactors. Scanning electron microscopy and energy-dispersive x-ray spectroscopy, and x-ray diffraction were used to study the morphology and

elemental compositions present in the hematite and promoted hematite oxygen carriers prior to and following the multi-cycle chemical looping reaction. The incorporation of 5 wt% MgO led to an increased reaction rate and an increase in oxygen utilized as compared to the pure hematite oxygen carrier. Possible reasons for the promotion effect by MgO were evaluated. These studies reveal that the best performing oxygen carrier was the 5 wt% MgO/Fe_2O_3 which exhibited no observed degradation in the kinetics and conversion performance in the methane step over 15 reduction and oxidation cycles. The Mg promoted oxygen carrier also showed reduced coke formation as compared to the pure hematite carrier.

Keywords: chemical looping, fluidized bed, fixed bed, MgO promoted hematite

1.0 Introduction

Chemical looping combustion (CLC) involves a two-step process in which a metal oxide (M_xO_y) oxygen carrier is used to transport oxygen to the fuel, avoiding direct contact between fuel and air. The CLC process has the advantage of producing sequestration-ready carbon dioxide (CO_2) without the energy penalty or need for nitrogen separation required by conventional combustion technology. The important properties of oxygen carriers are the high reactivity for reduction and oxidation as well as high mechanical stability during the multi-cycle testing.

Oxygen carrier development is critical for CLC where Fe_2O_3 has commonly been used as an oxygen carrier. Iron oxide has been known to show a slow reaction rate with CH_4 and is a critical issue for Fe_2O_3-based carriers. It is also known that impregnated Fe_2O_3 on alumina exhibits high reactivity with CH_4. [1] Many efforts have been made to develop oxygen carriers for the CLC technology [2]. Carriers that have been attempted include metal oxides such as CuO [3-11], Fe_2O_3 [12-16], NiO [12, 17-20], Mn_3O_4 [21-23], or CoO [24] supported on materials such as CeO_2

[17, 25], Al_2O_3 [11, 18, 24, 26], $MgAl_2O_4$ [18, 19, 23, 27-29], SiO_2 [22, 23, 30], TiO_2 [31], ZrO_2 [32], stabilized ZrO_2 [19, 32], and bentonite clays [33, 34], for both gaseous (natural gas) and solid fuels (coal). The reaction of methane with the metal oxide oxygen carrier, shown in equation 1, occurs by the oxygen in the metal oxide reacting with methane to produce CO_2 and H_2O. Regeneration of the oxygen carrier, shown in equation 2, occurs when the reduced metal reacts with the oxygen in air to return the oxygen carrier to its oxidized state.

$$CH_4 + MeO \longrightarrow CO_2 + Me + H_2O \quad (1)$$

$$Me + O_2 \longrightarrow MeO \quad (2)$$

A suitable oxygen carrier should readily release oxygen to oxidize CH_4 to produce CO_2 and H_2O. To design a commercially acceptable CLC process, it is critical to improve the oxygen utilization and reactivity of metal oxide materials. Therefore, development of more efficient oxygen carriers capable of a higher oxygen transfer rate in CLC of gaseous fuels is necessary. The oxygen carrier should exhibit high reactivity, capacity, high attrition resistance and cyclic stability during operation between 800–1000 °C. Avoiding carbon formation reactions by the reduced metal helps avoid the oxygen carrier deactivation process [35, 36]. In addition, the oxygen carrier should be inexpensive to manufacture and maintain.

Several pilot scale tests [14, 37-39] have been conducted using iron-based oxygen carriers, but reactivity improvements are still necessary for a cost-effective process. NiO-based oxygen carriers have shown promising results in pilot scale tests, but they cause environmental concerns. Generally in the literature [11, 15, 16, 18, 19, 22-24, 28, 29, 31, 34], improvement of the oxygen transfer ratio and reactivity are attributed to a well-dispersed metal oxide upon a suitable support material to achieve stable multi-cyclic reduction-oxidation performance during the CLC reaction. To achieve the desirable combination of properties, attrition resistance, resistance to chemical

attack, high strength, and high reactivity, researchers have combined iron oxide with Mg-bearing inert support materials with some success. Of these oxygen carriers, a carrier composed of Fe_2O_3 supported on $MgAl_2O_4$ shows high reactivity in the fluidized-bed reactor [40]. Other researchers have examined the optimal ratios of Fe_2O_3 (active) to $MgAl_2O_4$ (inert), as well as the most effective sintering temperatures and found that 60% Fe_2O_3 and 40% $MgAl_2O_4$ sintered at 1100 °C was the most suitable combination for an Fe-supported oxygen carrier [41]. In this work, we propose a new oxygen carrier using only 5 wt% MgO to promote the natural ore hematite with calcination temperature of only 800 °C.

Work on use of promoters to enhance the reactivity of metal oxide oxygen carriers is limited. Addition of 5 wt% NiO to Fe_2O_3 significantly improves fuel conversion during methane CLC [42]. Catalytic conversion of methane to reactive intermediates by reduced Ni was attributed to the improved performance of Fe_2O_3. Improvement in performance of illmenite has also been observed after addition of 5 wt% NiO [43]. Oxygen carriers prepared with NiO and $MgAl_2O_4$ also performed well [44]. Our previous research [45] also showed that the addition of 5 wt% ceria can enhance the reactivity of hematite significantly.

Our laboratory results indicate that 5 wt% MgO can enhance the performance of the natural ore hematite (Fe_2O_3) during CLC reaction, were the inert (MgO) does not merely act as a support in this work. A similar design for an oxygen carrier using MgO as a promoter to increase the oxygen utilization has not been reported in the literature, though several studies use MgO as a support material for Fe_2O_3, which required the amount of MgO greater than 25 wt% [46, 47].

The studies described in this study have demonstrated that the addition of a small amount of MgO (< 25%) to the hematite ore does not increase the surface area of the hematite carrier, but significantly enhances the oxygen utilization of the Fe_2O_3-based carrier. This reactivity enhancement decreases when the MgO content is 40%. These studies also indicate that MgO

promotes the CLC reaction and does not act as a support to the oxygen carrier. Our work demonstrates that the unsupported mixed metal oxide consisting of MgO-Fe_2O_3 has a specific composition that exhibits superior reactivity compared to the pure Fe_2O_3 oxygen carrier. While it does not exhibit agglomeration after multi-cycle operation, it does prevent sintering, and it reveals that the addition of small amounts of an MgO to Fe_2O_3-based carriers results in highly reactive oxygen carriers in the CH_4 CLC process. The superior reactivity enables the novel oxygen carrier to react with gaseous fuels and increases methane conversions, which may contribute to lowering the operating cost of the chemical looping combustion process.

The purpose of this work is to assess the performance of the MgO-promoted hematite as compared to hematite under thermogravimetric analysis and in the fluidized-bed reactor. Characterization of the oxygen carrier using SEM-EDS and XRD analysis coupled with lab-scale flow reactor tests, and bench-scale fixed-bed and fluidized-bed reactor tests at 800 and 900 °C were also conducted.

The chemical looping process is designed to produce heat and steam that could be used for various industrial applications. The power generation requires temperatures greater than 1000 °C, whereas, the CLC reaction between 800 and 900 °C is suitable to generate steam for such applications as extracting heavy oils from tar sands. The choice of 800 °C to study the oxygen carrier reactivity reported in the current work places the application of this oxygen carrier within the temperature regime that is best suited for low-temperature steam industrial applications.

2.0 Experimental Section

2.1 Materials and Oxygen Carrier Preparation

The Michigan hematite used for these studies was obtained from Ward's Natural Science (Rochester, NY). The purge gas between the oxidation and reduction cycles was Grade 2.0 helium and/or argon from Butler Gas Products Co. Inc. The UHP-grade CH_4 was during reduction from Matheson Tri-gas. The Grade 2.0 air was used for the oxidation cycle from Butler Gas Products Co. Inc.

The oxygen carrier preparations are described elsewhere [45, 48]. The 5 wt% and 25 wt% MgO-promoted hematite oxygen carriers were prepared using commercial $Mg(OH)_2$ (Aldrich), dolomite (Aldrich), and magnesium nitrate (Aldrich). Weight percentages reported here are based on MgO derived from various precursors, such as $Mg(OH)_2$ and Mg-nitrate. The pure MgO material was obtained by calcining the $Mg(OH)_2$ in a furnace at 800 °C. For comparison purposes, 5 wt% and 25 wt% Al_2O_3/hematite were also prepared by the impregnation method. Following calcination at 800 °C for 3 hours, the oxygen carrier samples were sieved to 100–300 microns. The BET surface area and pore size of the oxygen carriers were measured using a Micromeritics ASP-2020 instrument.

X-ray diffraction (XRD) analysis was carried out using a Panalytical PW 3040 X-Pert Pro SRD system equipped with a 60 kV PW 3373/00 3011/20 detector. The x-ray wavelength used was Cu Kα-1 at 1.54056Å The maximum resolution was 0.003° (2θ). System calibration was carried out using a polysilicon pressed disk with the Si(111) referenced to 28.443° (2θ). Sample data was acquired at 40 kV and 45 m Áin a line-focus mode using a standard PW3071/60 powder diffraction stage. XRD patterns of the fresh and following 15 redox cycles were collected at room temperature.

2.3 Scanning Electron Microscope Energy-Dispersive X-ray Spectroscopy Analysis

Scanning electron microscope (SEM) energy-dispersive x-ray spectroscopy analysis was conducted using a JEOL 7600 FESEM system interfaced to a Thermo-Electron System 7 microanalysis system. The Thermo-Electron microanalysis system is equipped with a Thermo-Electron Ultradry Energy Dispersive Spectrometer (EDS) and an EDAX Electron Backscatter Diffraction system.

2.4 Thermo-gravimetric Analysis

Thermo-gravimetric analysis (TGA) was conducted in a TA Instruments model 2050 thermo-gravimetric analyzer. The samples were placed in a 5-mm deep and 10-mm diameter crucible. Approximately 85 mg of the metal oxide oxygen carrier was heated from ambient temperature to 800 °C at a heating rate of 10 °C/min under N_2 gas at a flow rate of 100 cm^3/min. The sample temperature was maintained isothermally for 20 minutes prior to the multi-cycle testing. The reaction gases used during reduction were 20% CH_4/balance N_2, and air during oxidation, a total flow rate of 100 cm^3/min. The weight change for the fully oxidized and reduced samples was used for calculating the oxygen utilization of the oxygen carriers.

The mass-based reduction rate was determined from the thermogram profile during the reduction cycle and converting the data to the fractional reduction (X) defined by equation 3.

$$X = \frac{M_o - M}{M_o - M_f} \qquad (3)$$

Where M is the instantaneous weight of the metal oxide, M_o is the initial weight before reduction, and M_f is the final weight of the carrier after reduction for 30 minutes. The mass-based reduction rate was calculated by differentiating the polynomial equation, according to equation 4.

$$Global\ Rate = \frac{dX}{dt} \qquad (4)$$

2.5 Fixed-Bed Lab-Scale Flow Reactor Study

The CLC studies were carried out using a Micromeritics Autochem HP lab-scale quartz reactor. The fixed-bed lab-scale flow reactor was operated in continuous flow mode where 1.0 g of sample was placed in the quartz glass reactor. The reactor effluent was analyzed using a Pfeiffer Omnistar™ mass spectrometer for the molecular ion responses corresponding to CH_4 (*m/z = 16*), H_2O (*m/z = 18*), CO (*m/z = 28*), O_2 (*m/z = 32*), Ar (m/z = 40), and CO_2 (*m/z = 44*). The inlet flow of 100% Ar was maintained at a total flow rate of 60 cm^3/min (space velocity 9000 h^{-1}) over the oxygen carrier at 101.3 kPa, while heating from 25 to 800 °C at a heating rate of 10 °C/min. The reactor temperature was maintained at 800 °C during the oxidation (air, 60 cm^3/min, 30 minutes) and reduction (20% CH_4/balance Ar, 60 cm^3/min, 30 minutes) cycles.

2.6 Fluidized-Bed Flow Reactor Study

The oxidation and reduction studies were carried out using a fluidized-bed reactor manufactured by Autoclave Engineers HR-160 Reactor Assembly (Model # 5010-2377/HR-160). The column height of is 35.4 cm, and the diameter is 6 cm. The reactor column is made from Inconel SB-564 to withstand temperatures up to 900 °C and reacting gas-solid flows. A ceramic porous plate with 15–40 μm pores is used as the gas distributor. The setup is equipped with three electrical heaters installed around the reactor to heat the reactor to the target temperature of 800 °C. Methane in Ar was used for reduction at a flow velocity of 7.8, which is twice the minimum fluidization velocity.

After the reduction reaction was completed (5 min), the system was purged with Ar, and air was introduced for 15 min. The reactor effluent was monitored using a Pfeiffer Omnistar mass spectrometer for the molecular ion responses corresponding to CH_4 (*m/z = 16*), H_2O (*m/z = 18*), CO (*m/z = 28*), O_2 (*m/z = 32*), He (m/z = 4), and CO_2 (*m/z = 44*). The inlet flow of 100% Ar was

maintained at a total flow rate of 7.8 LPM (space velocity 2293 h^{-1}) over the oxygen carrier at 111.3 kPa, while heating from 25 to 800 °C at a heating rate of 4 °C/min. The reactor temperature was maintained at 800 °C during the oxidation (3.9 LPM Air + 3.9 LPM Ar, 15 min) and reduction (5 % Vol CH_4 balance Ar) cycles. Integrated molecular ion peaks for CH_4, CO_2, CO, and O_2 were used for calculating the amount of these species during the CLC reaction.

3.0 Results

3.1 XRD and SEM-EDS Characterization of the OC Materials

XRD analysis was performed on the promoted hematite oxygen carrier before and after 15 oxidation and reduction cycles at 800 °C. The XRD diffraction patterns following 15 redox cycles of the 5% and 25% MgO(nitrate)/hematite, dolomite/hematite, and MgO($Mg(OH)_2$)/hematite are shown in Figures 1a, 1b, and 1c respectively. For comparison, XRD data for pure Fe_2O_3, MgO, and dolomite are also shown in Figure 1.

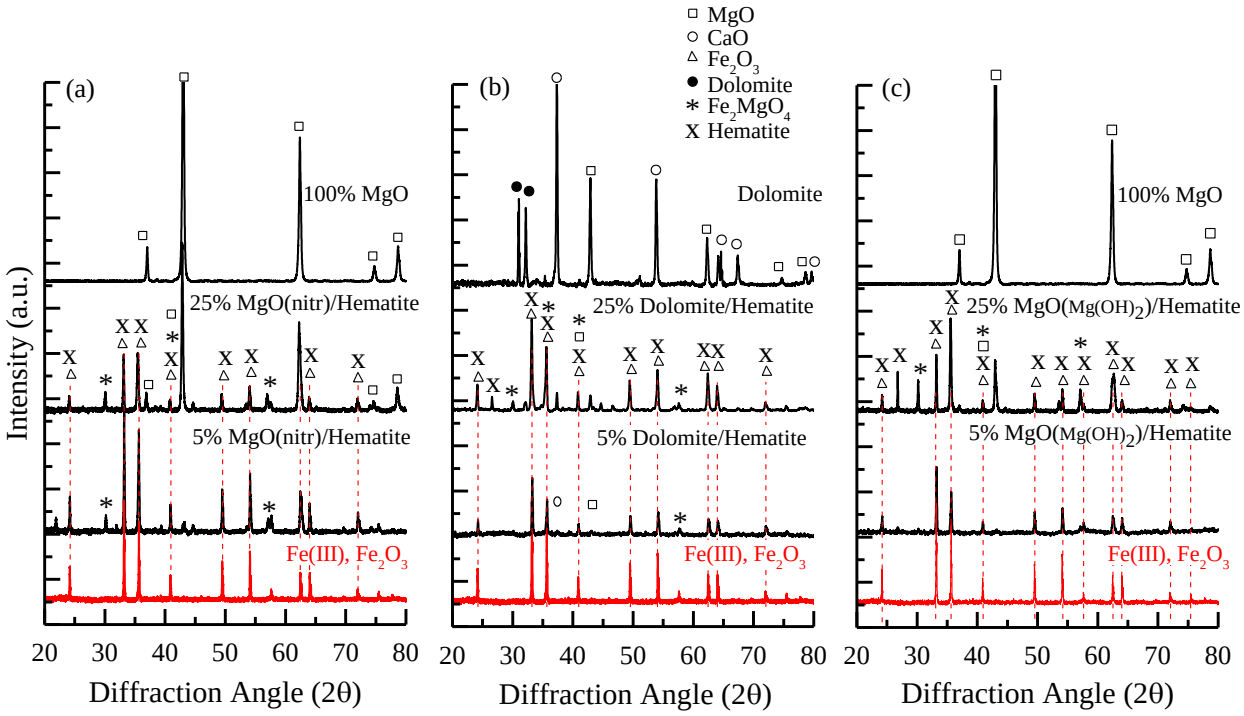

Figure 1. X-ray diffraction patterns following 15 redox cycles at 800 °C for (a) 5% and

25% MgO(nitrate)/hematite, pure Fe_2O_3, and MgO, (b) 5% and 25% dolomite/hematite, pure Fe_2O_3, and pure dolomite, and (c) 5% and 25% MgO($Mg(OH)_2$)/hematite, and pure Fe_2O_3 and MgO.

The pure MgO diffraction pattern shows five strong peaks at 36.8°, 42.8°, 62.2°, 74.5°, and 78.5° (PDF: 01-079-0612, MgO database) shown in Figures 1a and 1c. The pure hematite diffraction pattern shows nine strong peaks at 24.1°, 33.1°, 35.6°, 40.8°, 49.4°, 54.1°, 62.4°, 64.0°, 72.0° (PDF: 01-073-2234, hematite database) shown in Figure 1. Inductively coupled plasma mass spectroscopy (Galbraith Laboratories) and material safety data sheets data indicated that 99% of hematite is Fe_2O_3. The phases identified following 15 redox cycles on the promoted hematite OCs are MgO, Fe_2O_3, and $MgFe_2O_4$, which are similar to the XRD patterns of unreacted fresh samples. The presence of Fe_2O_3 in the reacted samples indicates that the OC could be re-oxidized in the presence of MgO following the cyclic methane oxidation CLC reactions.

The XRD diffraction patterns indicate some formation of $MgFe_2O_4$ [49], and MgO and Fe_2O_3 were also observed. The XRD data indicates that only a fraction of MgO and Fe_2O_3 reacted to form $MgFe_2O_4$, regardless of the type of Mg-precursor material that was used in the preparation after having sintered at 800 °C for 3 hours, shown in Figures 1a, 1b, and 1c. Because the initial calcination temperature and the reaction temperature were relatively low (800 °C), the majority of MgO remained as MgO without forming other compounds with Fe_2O_3.

SEM-EDS imaging (not shown) of the fresh and used 5% MgO/hematite revealed that the MgO remained evenly dispersed over the hematite material. Even dispersion of MgO on hematite is important for improving the reactivity of the OC hematite carrier.

3.2 Oxidation-Reduction Experiments in the Lab-Scale Reactor

The data in Figure 2 illustrates the outlet concentrations (moles) of CO_2 and CO per 100 g of carrier as a function of the reduction cycle at 800 °C for hematite containing both 5 wt% and 25 wt% compositions of MgO derived from Mg-nitrate, dolomite, and $Mg(OH)_2$. For comparison, the data for 5 wt% and 25 wt% Al_2O_3/hematite oxygen carriers and pure hematite are also shown in Figures 2a and 2b respectively. The 15-cycle chemical looping reduction and oxidation data demonstrates the stability of the oxygen carriers during the multi-cyclic testing. Mass spectroscopic analysis of the reactor effluent indicated that the reactivity of the OCs slightly increased with the number of cycles for both the hematite and the promoted hematite oxygen carriers. Table 1 summarizes the moles of CO_2 and CO and the percentage of O_2 used per 100 g carrier during the lab-scale reactor tests conducted at 800 °C. The pure hematite produced 0.17 mol CO_2 on the 15^{th} reduction cycle. The addition of 5% MgO to the hematite increased the amount of CO_2 produced to 0.32 mol on the 15^{th} cycle, which corresponds to an increase in the amount of CO_2 produced by 1.9 times for the MgO-promoted hematite, as compared to the pure hematite.

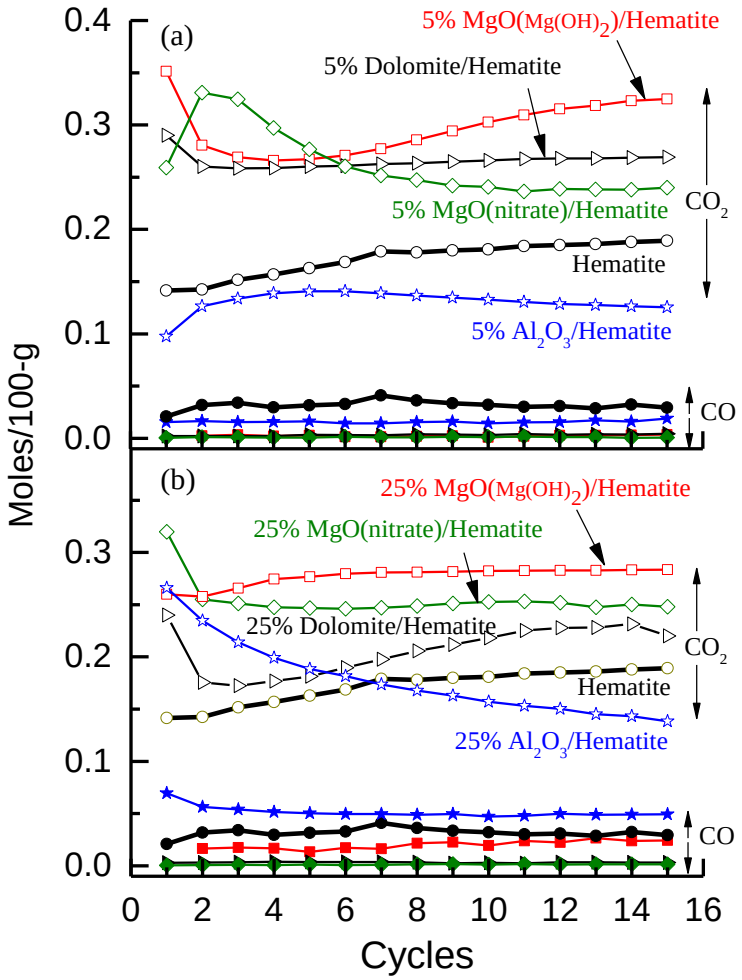

Figure 2. The amount of CO_2 (open symbols) and CO (closed symbols) produced during the reduction cycles flowing 20% CH_4/He at 800 °C, over (a) 5% dolomite/hematite, 5% MgO($Mg(OH)_2$)/hematite, 5% MgO(nitrate)/hematite, and 5% Al_2O_3/hematite and hematite, and (b) 25% dolomite/hematite, 25% MgO($Mg(OH)_2$)/hematite, 25% MgO(nitrate)/hematite, 25% Al_2O_3/hematite, and pure hematite oxygen carriers.

Table 1. Moles CO_2, CO produced during CH_4 reduction and percentage O_2 utilized during oxidation per 100g carrier during the lab-scale reactor tests at 800 °C.

	Moles CO_2/100-g	**Moles CO/100-g**	**% O_2 Utilized**

Carrier	Cycle 2	Cycle 15	Cycle 2	Cycle 15	Cycle 15	S
100% MgO	0.018	0.011	0.0048	0.002	-	-
100% Dolomite	0.061	0.064	0.016	0.012	-	-
Hematite	0.14	0.17	0.032	0.032	4.5	84.2
5% Al_2O_3/Hematite	0.12	0.12	0.017	0.019	3.3	86.3
5% MgO($Mg(OH)_2$)/Hematite	0.28	0.32	0.002	0.004		98.7
5% MgO(nitrate)/Hematite	0.32	0.24	0.001	0.006	6.1	99.7
5% Dolomite/Hematite	0.25	0.26	0.002	0.004	6.6	98.6
25% Al_2O_3/Hematite	0.23	0.13	0.06	0.05	4.9	73.4
25% MgO($Mg(OH)_2$)/Hematite	0.25	0.28	0.003	0.003	9.0	98.9
25% MgO(nitrate)/Hematite	0.25	0.24		0.001	7.7	99.4
25% Dolomite/Hematite	0.18	0.22	0.02	0.02	7.4	90.1

The presence of MgO also improved the CO_2 selectivity during the CL reaction. The pure hematite produced 0.03 mol CO on the 15th reduction cycle, shown in Figure 2a. The addition of 5% MgO by $Mg(OH)_2$, dolomite, and Mg-nitrate decreased the amount of CO produced to 0.004, 0.004, and 0.006 moles respectively. For comparison, a 5% Al_2O_3/hematite carrier was prepared and tested for 15 reduction and oxidation cycles. The data in Figure 2a indicates that the addition of 5% Al_2O_3 decreases the amount of CO_2 produced as compared to that with hematite. The decrease in CO_2 production, upon the addition of 5% Al_2O_3 and as compared to the MgO, suggests that Al_2O_3 does not participate in promoting the combustion of CH_4. BET surface area data indicated that the addition of Al_2O_3 or MgO did not increase the surface area (5 wt% MgO/hematite < 1.0 m^2/g) of the oxygen carrier, as shown in Table 2. Thus, the improvement in oxygen carrier utilization upon addition of MgO, during the CH_4 CLC reaction, has to occur by a mechanism other than surface area enhancement.

Table 2. BET surface areas and pore size of the prepared oxygen carriers.

Carrier	Fresh (m^2/g)	Reacted[a] (m^2/g)	Fresh Pore Size[b]	Reacted[a] (Å)
MgO (hydroxide)	13.3	-	99.9	-
MgO (nitrate)	4.1	-	193.2	-
Dolomite	< 1.0	-	136.1	-
Fe_2O_3 (Hematite)	< 1.0	< 1.0	63.6	79.7
5% Al_2O_3/Fe_2O_3	1.3	< 1.0	67	-
25% Al_2O_3/Fe_2O_3	1.6	< 1.0	129.4	-
5% MgO(nitrate)/Fe_2O_3	< 1.0	< 1.0	150.9	162.1
25% MgO(nitrate)/Fe_2O_3	2.6	1.4	206.1	182.4
5% MgO(hydroxide)/Fe_2O_3	< 1.0	< 1.0	290.8	141.0
25% MgO(hydroxide)/Fe_2O_3	4.1	1.4	306.1	219.6
5% Dolomite/Fe_2O_3	< 1.0	< 1.0	689.5	161.8
25% Dolomite/Fe_2O_3	1.6	< 1.0	567.3	196.2

[a] *Reaction temperature 800 °C*
[b] *Freshly prepared materials*

The 25 wt% MgO/hematite oxygen carrier (Figure 2b) produced 0.28 mol CO_2 and 0.003 mol CO at 800 °C. This indicated that increasing the loading of MgO to 25% from 5% (Figure 2a) decreased the amount of CO_2 produced, which could result from the decrease in the amount of Fe_2O_3 present. The 25 wt% MgO($Mg(OH)_2$)/hematite produced more CO_2 than the 25 wt% dolomite and MgO(nitrate)-promoted hematite. Similar results were observed for the 5 wt% MgO-promoted hematite: the $Mg(OH)_2$ outperformed the dolomite and MgO(nitrate)-promoted carriers. In addition, increasing the amount of MgO loading above 5 wt% did not significantly increase the amount of CO produced. For comparison, 25 wt% Al_2O_3/hematite carrier was also tested, and the data revealed that increasing the Al_2O_3 loading to 25 wt% increased the amount of

CO_2 produced to 0.23 mol CO_2 (from 0.12 mol CO_2 on 5 wt% Al_2O_3/hematite) on cycle 2. However, this amount was lower than the amount of CO_2 produced from the 25 wt% MgO/hematite carriers. Following multiple redox cycles, the 25 wt% Al_2O_3/hematite shows significant deactivation; the oxygen utilization at the end of the 15 reduction cycles was less than that of the pure hematite carrier.

When the methane CLC reaction was performed with pure MgO, the amounts of CO_2 and CO produced were significantly lower than that with hematite, as shown in Figure 3, indicating that MgO is not reactive for total oxidation of methane during the CLC reaction. MS analysis indicated that the addition of 5% MgO to the hematite oxygen carrier increased production of CO_2 per unit time by 1.9 times, as compared to the sum of the CO_2 produced per unit time when hematite and Mg oxides are tested separately. Thus the presence of MgO alone in the MgO/hematite carrier is not sufficient to account for the significant increase in CH_4 combustion.

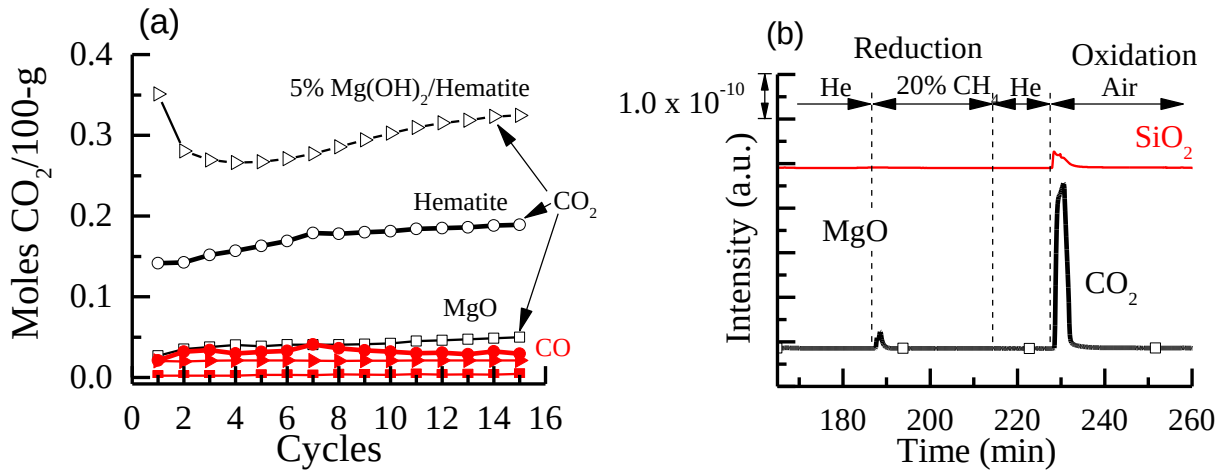

Figure 3. Amount of CO_2 produced during (a) reduction cycles flowing 20% CH_4/He at 800 °C over pure MgO, 5% MgO/hematite, and hematite oxygen carriers, and (b) one reduction and oxidation cycle at 800 °C in the lab-scale reactor with MgO and SiO_2.

Figure 3b shows the MS analysis of the reactor effluent during one reduction and oxidation cycle at 800 °C in the lab-scale reactor. The MS intensity data in Figure 3b for the pure MgO shows low reactivity for both CO_2 and CO formation during the reduction cycle. During the oxidation cycle, however, a large amount of CO_2 was observed, suggesting that CH_4 decomposition to carbon occurred on the MgO surface, which led to its oxidation to CO_2 during the oxidation cycle. For comparison, pure SiO_2 was tested for 15 reduction and oxidation cycles. The results indicate that SiO_2 was unreactive for CO_2 formation during reduction, and there was minimal decomposition of CH_4 to carbon, as indicated by the small amount of CO_2 produced during the oxidation cycle. These results indicate that the unique promotion effect of MgO, may be facilitated by the CH_4 decomposition over the MgO to form carbon and H_2, which may be intermediates for the reaction with Fe_2O_3.

The percentage oxygen utilized was determined using the MS data for CO_2 and CO during the CL reduction cycles at 800 °C. The percent oxygen utilized (calculated by equation 5) during the 15th reduction cycle for the 5 and 25 wt% MgO/hematite oxygen carriers are shown in Table 1.

$$Percentage\,O_2\,Utilized = \frac{n_{O2}}{n_{O2}\left(Theoretical\right)} \qquad (5)$$

where n_{O2} is the moles of oxygen used during the reduction reaction to form CO and CO_2. n_{O2}(theoretical) is the theoretical total amount of oxygen available in the oxygen carrier. The amount of oxygen used on the pure hematite carrier, during a 30-minute reduction time, on the 15th reduction cycle was 4.5% O_2 (Table 1). The addition of 5% MgO, by impregnation of $Mg(OH)_2$, to the hematite material resulted in an increase in O_2 utilization to 8.1% as compared to the pure hematite. Adding 5% Al_2O_3 to hematite did not have any significant impact on oxygen utilization of the hematite.

The surface area increase on addition of 5 wt% MgO via nitrate, hydroxide, and dolomite was minimal (as shown in Table 2), yet the increase in oxygen utilization (Table 3) was

significant, indicating the mechanism of promotion by MgO is not due to surface area enhancement. The 25 wt% MgO/hematite carriers, listed in Table 1, also show an improvement in the amount of oxygen utilized during the reduction cycle. The 25 wt% Al_2O_3/hematite (Figure 2b and Table 1) showed 8.2% O_2 utilization in cycle two, but a significant deactivation occurred over 15 cycles that resulted in 4.9% oxygen utilization, which is similar to that of the pure hematite carrier but higher than that for 5 wt% Al_2O_3/hematite carrier. In contrast, the addition of 25 wt% MgO to hematite improved the oxygen utilization of hematite and was stable during the 15-cycle testing. MgO derived from different precursors improved the performance of hematite and CO_2 selectivity. The $Mg(OH)_2$-impregnated hematite showed greater reactivity than the magnesium nitrate and dolomite-promoted hematite carriers. The results of the lab-scale reactor study demonstrated significant enhancement of the reactivity and oxygen availability of hematite carriers by the addition of the MgO regardless of the MgO precursor material. MgO has a unique effect on promoting the performance of Fe_2O_3.

Table 3. Oxygen transfer ratio (R_o) of the oxygen carriers.

			R_o				
Carrier	**Fuel**	**Reactor**	**(750 °C)**	**(800 °C)**	**(900 °C)**	**CO_2 Sel.**	**Refs.**
Hematite	20% CH_4/N_2	Fix bed	0.018	0.027	0.06	84.2[A]	This work
Hematite	5% CH_4/N_2	Fluid bed	-	0.02	-	71.4[A]	This work
5% MgO($Mg(OH)_2$)/Hematite	20% CH_4/N_2	Fix bed	0.014	0.080	0.14	99.4[A]	This work
25% MgO($Mg(OH)_2$)/Hematite	20% CH_4/N_2	Fix bed	0.010	0.084	0.12	99.4[A]	This work
5% MgO($Mg(OH)_2$)/Hematite	5% CH_4/N_2	Fluid bed	-	0.045	-	86.9[A]	This work
5% Dolomite/Hematite	20% CH_4/N_2	Fix bed	0.017	0.052	0.066	99.4[A]	This work
25% Dolomite/Hematite	20% CH_4/N_2	Fix bed	0.022	0.051	0.065	95.4[A]	This work
5% MgO(Nitrate)/Hematite	20% CH_4/N_2	Fix bed	0.013	0.051	0.1	99.9[A]	This work

25% MgO(Nitrate)/Hematite	20% CH_4/N_2	Fix bed	0.032	0.044	0.077	99.7[A]	This work
5% CeO_2/Hematite	20% CH_4/N_2	Fix bed	0.024	0.037	0.11	90[A]	[45]
25% CeO_2/Hematite	20% CH_4/N_2	Fix bed	0.031	0.042	0.14	79[A]	[45]
40% CuO/20% Fe_2O_3/Al_2O_3	20% CH_4/N_2	TGA		0.14	0.14	-	[50]
Fe_2O_3–CuO/Al_2O_3	3% H_2/Ar	TGA	0.186	0.205	0.225	-	[3]
45%Fe_2O_3/Al_2O_3	15% CH_4	Fluid bed			0.013[B]	-	[15]
60% Fe_2O_3/Al_2O_3	88% CH_4	Fluid bed			0.031[B]	70[B]	[51]
15% Fe_2O_3/Al_2O_3	25% CH_4	Fluid bed			0.015[B]	50[B]	[1]
40%NiO/Al_2O_3	15% CH_4	Fluid bed			0.084[B]	-	[15]
10% CuO/Al_2O_3	15% CH_4	Fluid bed			0.02[B]	-	[15]
40% $NiO/MgAl_2O_4$	50% CH_4, 50% H_2O	Fluid bed			0.045[B]	90[B]	[52]
18% NiO/Al_2O_3	30% CH_4/N_2	TGA, Fluid bed			0.038[B]	60[B]	[53]

[a] 800 °C reaction temperature

[b] 950 °C reaction temperature

3.3 Reactivity of the Oxygen Carriers Investigated by TGA

An important characteristic of the oxygen carrier is the oxygen utilization, also called the oxygen ratio, defined as $R_o = (m_{ox} - m_{red}) / m_{ox}$, where m_{ox} and m_{red} are the masses of the oxidized and reduced forms of the metal oxide, respectively. The weight change during thermogravimetric analysis of the promoted hematite and pure hematite oxygen carriers was used for calculating the oxygen ratio of the prepared oxygen carriers. The oxygen ratio during the reduction cycles while flowing 20% CH_4/He at 800 °C, over the 5 wt% dolomite/hematite, 5 wt% MgO($Mg(OH)_2$)/hematite, 5 wt% MgO(nitrate)/hematite, and pure hematite are shown in Figure 4a. The oxygen ratio for the 25% dolomite/hematite, 25% MgO($Mg(OH)_2$)/hematite, 25%

MgO(nitrate)/hematite, and 25% Al_2O_3/hematite, and pure hematite oxygen carriers are shown in Figure 4b.

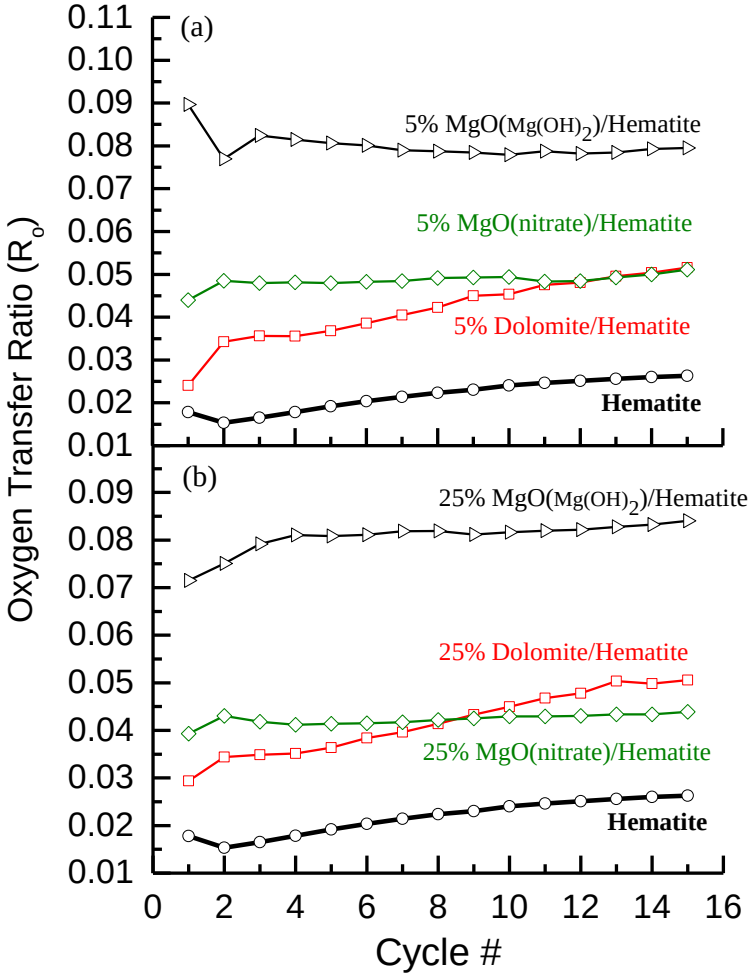

Figure 4. Oxygen utilization during the reduction cycles flowing 20% CH_4/He at 800 °C, over (a) 5% dolomite/hematite, 5% MgO($Mg(OH)_2$)/hematite, 5% MgO(nitrate)/hematite, and pure hematite, and (b) 25% dolomite/hematite, 25% MgO($Mg(OH)_2$)/hematite, 25% MgO(nitrate)/hematite, and pure hematite oxygen carriers.

The oxygen ratio during 20 minutes of reduction for the pure hematite oxygen carrier was 0.027 on the 15th reduction cycle. The addition of 5 wt% MgO to hematite by magnesium nitrate and dolomite increased the oxygen ratio to 0.052, whereas the $Mg(OH)_2$-promoted hematite

shows an oxygen ratio of 0.08. Increasing the loading of MgO to 25 wt% did not significantly increase the oxygen ratio. Increasing the reaction temperature from 800 to 900 °C significantly affected the rate of reaction and increased the oxygen ratio as compared to the pure hematite carrier, shown in Table 3. The oxygen ratio of the promoted Fe_2O_3 carriers is better than that reported for other iron-based carriers. [1, 15, 54]

Figure 5a illustrates the rate of mass conversion as a function of fractional mass conversion (ω) computed for the 2nd reduction cycle at 800 °C from TGA data for the 5 wt% MgO-promoted hematite and pure hematite oxygen carriers.

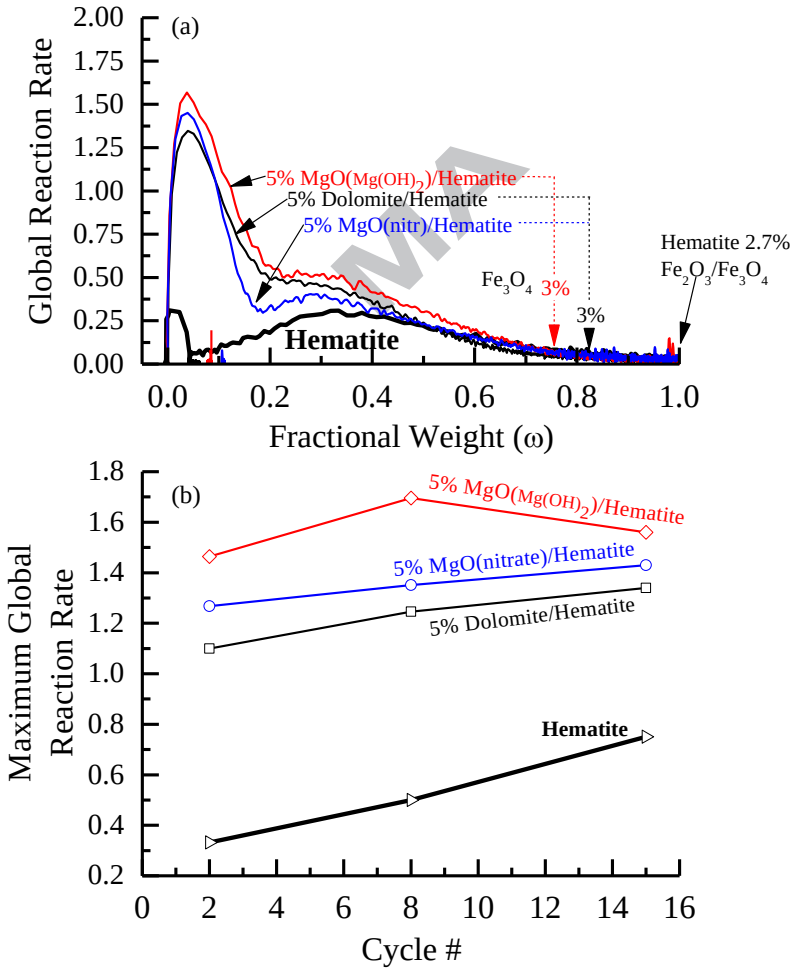

Figure 5. Reaction rates from TGA data at 800 °C as a function of (a) the mass-based conversion and (b) cycle number.

The pure hematite oxygen carrier showed a significantly lower reduction rate (0.30 min^{-1}-maximum) than MgO-promoted hematite. The rates of reaction for hematite and promoted hematite as a function of cycle number are shown in Figure 5b, for reduction cycles 2, 8, and 15, and the data indicates that the reactivity of both hematite and promoted hematite increased slightly with the increasing number of reduction cycles.

The TGA thermogram profile for hematite showed only a 2.7% decrease in the carrier weight, following the 20-minute reduction, indicating that Fe_2O_3 was not fully converted to Fe_3O_4 during the 20-minute reduction period. The promoted hematite exhibited an initial rapid reaction with CH_4, followed by a more gradual decrease in the rate at higher exposure times, shown in Figure 5a. This effect may be due to two kinds of reactions taking place during the reduction of the oxygen carrier or due to the reaction of surface and bulk oxygen. The weight change of greater than 3 wt% in the 20-minute reaction time with MgO-promoted hematite oxygen carriers indicates that the MgO improved the reducibility of the hematite material, converting all Fe_2O_3 to Fe_3O_4 in less than 20 minutes. Some Fe_3O_4 was also converted to FeO during this reduction period. Increasing the MgO loading on hematite did not significantly increase the reactivity of the oxygen carrier. The promotion effect of the MgO resulted in the conversion of Fe_2O_3 to Fe_3O_4 in a shorter reaction time, as shown in Figure 5a. The type of MgO precursor also had an effect on the rate as follows: MgO(hydroxide) > MgO(nitrate) > MgO(dolomite) > hematite. The corresponding reaction rates were 1.57 min^{-1}, 1.44 min^{-1}, and 1.34 min^{-1} respectively.

To investigate whether the promotion effect by MgO is unique to the reaction with methane, TGA tests were also conducted with other reducing gases. Figure 6 illustrates a comparison of the oxygen ratio during fifteen reduction cycles in the TGA using 20% H_2/N_2 and 20% CH_4/N_2 at 800 °C over the 5 wt% MgO/hematite and pure hematite. The data indicates that both the MgO/hematite and pure hematite oxygen carriers show a similar oxygen ratio under H_2-reduction, with MgO/hematite having slightly higher utilization after 7 cycles. In contrast, the

promotion effect of MgO is more significant during the reaction with methane, indicating that MgO promotes a unique reaction mechanism with methane. Our previous carrier studies with CeO_2/hematite[45] indicated that CeO_2-promoted methane decomposition to form intermediates that are reactive for CLC. The MgO promotion effect may also be proceeding via a similar reaction mechanism.

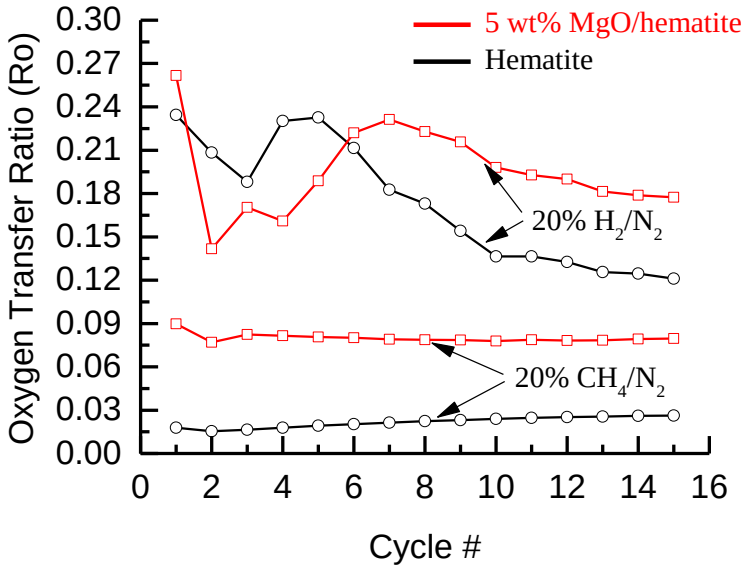

Figure 6. Oxygen utilization during the reduction cycles flowing 20% H_2/N_2 and 20% CH_4/N_2 at 800 °C over 5% MgO/hematite and pure hematite oxygen carriers.

The aim of the TGA and lab-scale fixed-bed experiments was to evaluate the reaction performance of the hematite and the MgO-promoted hematite materials using various MgO precursors and preparation techniques for application in larger-scale investigations. The results of these studies revealed that the $Mg(OH)_2$-promoted hematite exhibits the best performance properties for methane reduction. In addition, increasing the loading from 5 wt% to 25 wt% did not show any additional enhancements in either the rate or oxygen transport of the promoted oxygen carriers. Therefore, based on these results, the 5 wt% MgO derived from the

$Mg(OH)_2$/hematite oxygen carrier was chosen as the best promoted oxygen carrier to be used for further testing in the fluidized-bed reactor.

3.4 Oxidation-Reduction Testing in the Fluidized-Bed Bench-Scale Reactor

The attrition rates of the MgO-promoted oxygen carriers were tested using the ASTM 5757-11 Method, *"Determination of Attrition of FCC catalysts"* in which fines were collected and weighed after 1, 3, and 5 hours. The attrition of the ExxonMobil FCC Catalyst was used as a baseline to compare attrition resistance of CLC carriers. The attrition index percentage is defined by the total mass of fines elutriated, divided by the initial sample mass. The FCC Catalyst attrition index was measured to be 5.77% (1 hour), 15.14% (3 hours), and 24.84% (5 hours). The hematite was measured to be 0.75% (1 hour), 2.12% (3 hours), and 3.06% (5 hours), and the promoted hematite was 3.31% (1 hour), 4.48% (3 hours), and 6.60% (5 hours). The attrition resistance for the promoted hematite was higher than the natural ore hematite, and significantly lower than the FCC catalyst standard. XRD analysis of the fines, from the promoted hematite OC, revealed both the MgO and Fe_2O_3 phases.

Evaluation of the MgO-promoted hematite for CH_4 CLC reaction was performed in a bench-scale fluidized-bed reactor. Gas with a composition of 5% CH4/balance-Ar at 800 °C was used during the reduction, and 50% air/balance-Ar was used during oxidation. The methane conversion (Figure 7a) and the outlet gas concentration profiles for CO and CO_2 (Figure 7b) for hematite and MgO-promoted hematite was determined using MS analysis. The oxygen utilization was calculated from the oxidation products CO and CO_2 (Figure 7c). The pure hematite showed a methane conversion of approximately 32% throughout the 15 cycle tests. Addition of MgO to hematite caused an increase in CH_4 conversion to 55% for the first 5 cycles. A slight deactivation to 45% was observed at the 6^{th} cycle, but it remained stable through the remainder of the reduction cycles.

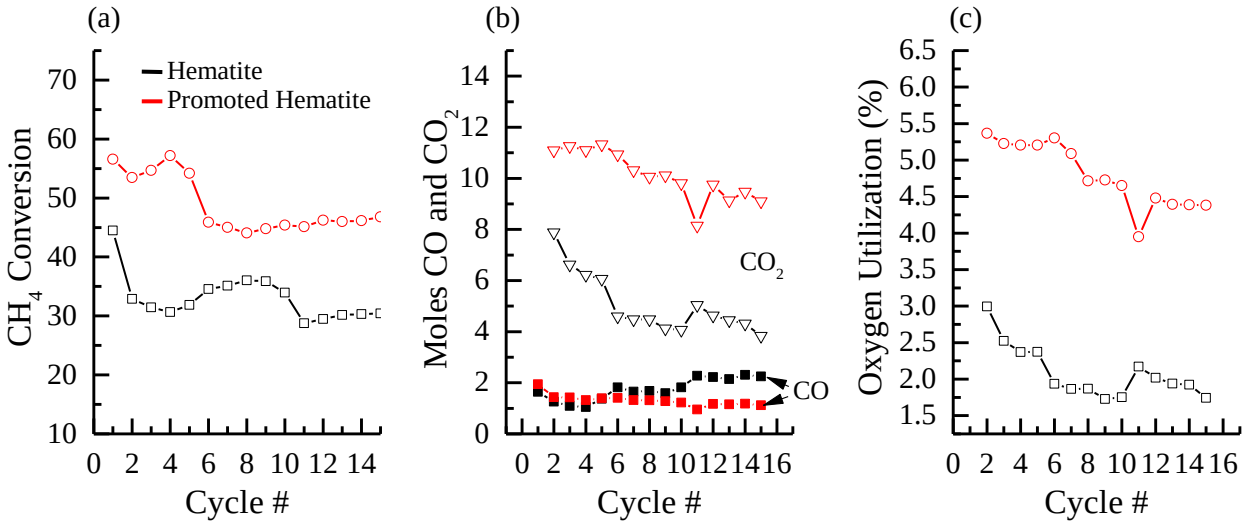

Figure 7. Fluidized-bed reactor data for (a) CH_4 conversion, (b) moles of CO_2 and CO produced, and (c) oxygen transfer capacity, during reduction cycle in 5% CH_4/N_2, at 800 °C.

The pure hematite produced 7.9 moles CO_2 and 1.8 moles CO on the second cycle. The amount of CO_2 produced decreased to 4 moles on the 15th cycle, and the amount of CO increased to 2 moles. The addition of MgO to hematite improved the amount of CO_2 produced (11.1 moles on cycle 2) as compared to the pure hematite (7.9 moles). The MgO-promoted hematite showed a decreasing trend of CO production with increasing number of cycles. Analysis of the combustion products CO and CO_2 indicated that the oxygen utilization was approximately 1.75% for the pure hematite on the 15th cycle. The presence of MgO increased the amount of oxygen utilized to 4.5% on the 15th cycle, which is an enhancement of 2.6 times in carrier performance as compared to the pure hematite carrier. The MgO promotion effect in the fluidized-bed tests is consistent with the bench-scale fixed-bed studies.

4.0 Discussion

Our experimental data with the TGA and fluidized-bed reactor studies clearly showed that the addition of 5–25% MgO to hematite improved the oxygen transfer capacity, reaction rates, and

methane percent combustion for the reaction with methane. Our previous kinetic analysis of TGA data [55] indicated that the reaction mechanism of methane-hematite changes after incorporation of MgO. In addition to this, when CH_4 was introduced to pure MgO, a negligible amount of CO_2 and CO were produced during reduction (Figure 3a), and a large amount of carbon was produced (Figure 3b) as evidenced by the CO_2 formation during oxidation. The oxygen utilization of MgO is near zero for methane reduction, suggesting MgO does not directly participate in the CLC reaction.

MgO could enhance the oxygen transfer capacity and reactivity of hematite with methane in several ways:

1. Enhancement of pore structure by MgO
2. MgO acting as support
3. Modification of the bulk structure of Fe_2O_3 by MgO
4. Enhancement of formation of reaction intermediates by MgO for methane combustion that facilitate the formation of reaction products.

Enhancement of the pore structure of hematite by MgO—The average pore size, measured from N_2 sorption data, is shown in Table 2. Based upon the N_2 sorption data, the average pore size significantly increased when MgO was incorporated with the hematite ore. The increase in reactivity of MgO/hematite carriers may be partially related to the increase in pore size of hematite after the addition of MgO. However, the highest increase in pore size was observed with dolomite, whereas the $Mg(OH)_2$-promoted hematite had the best reactivity. The 25% MgO/hematite samples also had larger pore sizes, but the 5% MgO/hematite still showed better performance. In addition, the reacted samples prepared with $Mg(OH)_2$ showed a lower pore size following a 15-cycle test, but the reactivity improved through the 15 cycles. Therefore, the

reactivity differences cannot be fully explained by the increase in pore size of the freshly prepared carriers.

MgO precursors had a larger pore size than Fe_2O_3. When MgO resides on the surface of the Fe_2O_3, the pore size measurements may reflect the pore size of MgO and not necessarily that of the MgO/Fe_2O_3 system. Thus, the diffusion limitation of Fe_2O_3 may not be affected by the pore size increase of MgO on the surface of the oxygen carrier. Note that MgO was incorporated into the natural hematite only after it was crushed to the desired size range, and MgO is more likely to reside on the surface of hematite. This is different from the incorporation of inert supports in oxygen carrier preparations in which both inert and metal oxide are initially mixed as fine powders before agglomerating to obtain the desired pellet sizes, and inerts will also reside in the bulk of the pellets.

MgO acting as a support—Because the amount of MgO required to show the promotion activity was approximately 5 wt%, and the surface area of hematite after incorporation of MgO did not increase, MgO is unlikely to act as a support to increase the reactivity of hematite. Generally, inert supports are used for better distribution of the active component to have better accessibility to the reactive gas. To achieve this, either the active component is deposited on the support or the support material (>25 wt%) is mixed well with the active component during the pellet preparations. Thus, most of the support resides in the bulk of the pellet not necessarily on the surface. In the current work, the MgO was impregnated on the hematite pellet, and most of the MgO may reside on the surface of the hematite pellet. The addition of 5 wt% alumina did not improve the reactivity of Fe_2O_3, which indicated that MgO has a unique promotion activity.

Modification of bulk structure by MgO—Previous work by Li et al. [56] has shown that the TiO_2 support can modify the bulk structure of Fe_2O_3 to enhance the oxygen release from Fe_2O_3. These oxygen carriers were prepared by mixing the TiO_2 powders with Fe_2O_3 powders prior to pelletization. Thus, TiO_2 is well mixed in the bulk structure with Fe_2O_3. The pellets were sintered

at 1200 °C for 48 hours. In the current work, MgO was added to the pellets of hematite natural ore (not prior to pelletization) and calcined at 800 °C for 3 hours. Structural changes in the bulk of the solid specifically due to lattice substitutions generally require high temperatures (>1100 °C), high solid-solid contacts in the bulk, and long calcination times. Because MgO resides mainly on the surface of hematite, and calcination was conducted for 3 hours at 800 °C, it is unlikely that lattice substitutions of bulk Fe_2O_3 can occur in the present work. Thus, it is not clear whether the improved oxygen ionic transfer mechanism can explain the enhanced reactivity of the Fe_2O_3 by MgO. In addition, if MgO improved the oxygen ionic transport of bulk hematite, it should also promote the reaction with H_2. However, a similar promotion effect was not observed during H_2 testing (Figure 6).

Enhancement of formation of reaction intermediates that facilitate the formation of reaction products by MgO—Our data indicated that MgO promoted the methane CLC reaction but not the H_2 CLC, as shown in Figure 6, which suggests that the promotion activity may be due to a modified reaction mechanism unique to methane. Catalytic decomposition of methane by transition metals, such as Ni, Co, and Fe [ ], are reported in the literature. Studies have shown that the incorporation of Mg in Ni catalysts increased the rate of methane decomposition [64]. The promotion of the decomposition of CH_4 may improve the oxygen transfer rate of Fe_2O_3 by interacting with reactive carbon-containing intermediate species. In our previous work [ ], the improvement in combustion performance was achieved by incorporation of CeO_2, which promoted the decomposition and partial oxidation of methane-producing carbon, CO, and H_2, which were reactive toward Fe_2O_3. The current data suggests that, unlike with CeO_2, partial oxidation of CH_4 does not occur on MgO. When the oxygen was introduced, following the reaction with methane, a significant amount of CO_2 was observed, as shown in Figure 3b, which indicated that MgO promotes methane decomposition similar to CeO_2.

In the absence of the MgO, methane appears to react directly with Fe_2O_3 to form CO_2 and CO via reactions 6–8. All of the reactions are thermodynamically favorable above 700 °C.

$$CH_4 + 12Fe_2O_3 \longrightarrow CO_2 + 8Fe_3O_4 + 2H_2O \qquad \Delta H^o_{r,800C} = 171.3 kJ/mol \qquad (6)$$

$$CH_4 + 3Fe_2O_3 \longrightarrow CO + 2Fe_3O_4 + 2H_2 \qquad \Delta H^o_{r,800C} = 221.1 kJ/mol \qquad (7)$$

$$CH_4 + Fe_3O_4 \longrightarrow CO + 3FeO + 2H_2 \qquad \Delta H^o_{r,800C} = 276.9 kJ/mol \qquad (8)$$

When MgO is present, it promotes CH_4 decomposition and may contribute to additional reactions (9–13) with Fe_2O_3, as shown below. These reactions are also thermodynamically favorable above 700 °C.

$$CH_4 \xrightarrow{MgO} C + H_2 \qquad (9)$$

$$2C + 7Fe_2O_3 \longrightarrow \frac{6}{3}CO + \frac{1}{3}CO_2 + \frac{24}{3}Fe_3O_4 \qquad \Delta H^o_{r,800C} = 248.1 kJ/mol \qquad (10)$$

$$2C + 3Fe_3O_4 \longrightarrow CO + CO_2 + 9FeO \qquad \Delta H^o_{r,800C} = 389.1 kJ/mol \qquad (11)$$

$$H_2 + 3Fe_2O_3 \longrightarrow H_2O + 2Fe_3O_4 \qquad \Delta H^o_{r,800C} = -5.3 kJ/mol \qquad (12)$$

$$H_2 + Fe_3O_4 \longrightarrow H_2O + 3FeO \qquad \Delta H^o_{r,800C} = -50.5 kJ/mol \qquad (13)$$

When Fe_2O_3 is present, the carbon and H_2 formed by MgO may react with Fe_2O_3 (Reactions 10–13) enhancing the overall methane CLC reaction.

X-ray diffraction analysis (Figure 1) revealed that the addition of MgO to Fe_2O_3 resulted in the some formation of $MgFe_2O_4$, but the most significant phases were MgO and Fe_2O_3 because the calcination temperatures were low (800 °C), and MgO was added to the surface of the hematite

pellets. Studies have shown that $MgFe_2O_4$ may also participate in the CL reaction (under 5% H_2), by releasing oxygen during reduction [49]. Our studies have shown that during the reaction with methane, the oxygen transfer capacity of $MgFe_2O_4$ is significantly lower than that with Fe_2O_3 (not shown). Assuming that all of the MgO added to the hematite formed $MgFe_2O_4$, 4% of the oxygen available may be derived from $MgFe_2O_4$.

Based upon the reactor tests, the addition of MgO to hematite resulted in an increase in O_2 use by 2X (Figure 7c) during the second cycle. The amount of O_2 available in the $MgFe_2O_4$ does not adequately explain the increase in O_2 utilization in the MgO-promoted hematite carrier, even if $MgFe_2O_4$ is more reactive than Fe_2O_3. The XRD data showed some of the MgO/Fe_2O_3 oxygen carriers remaining as the MgO and Fe_2O_3 phases following 15 oxidation and reduction cycles at 800 °C. Therefore, the high activity of the MgO/Fe_2O_3 carrier is most likely due to the cooperative participation of MgO sites, which produces intermediate species—carbon and H_2—that facilitate the further reduction of the Fe_2O_3 oxygen carrier, according to reaction steps 10 through 13. Previous work has shown that the addition of 5 wt% NiO to Fe_2O_3 significantly improved the fuel conversion during methane CLC [ ], and catalytic conversion of methane to reactive intermediates by reduced Ni was attributed to the improved performance of Fe_2O_3. Improvement in fuel conversion on NiO/alumina after addition of MgO has also being reported previously [ ], and the authors related this to the formation of $MgAl_2O_4$ at calcination temperatures of 1300–1600 °C, which is different from the present work.

In methane CLC, Fe_2O_3 gets reduced to states such as FeO and Fe that act as catalysts for carbon formation by catalytic decomposition of methane. In general, this carbon formation reaction is not favorable for the CLC process [33, 36] because this carbon cannot be oxidized due to unavailability of oxygen in the vicinity. In the present work, we propose that carbon formation takes place prior to reduction of Fe_2O_3 at the MgO site (Figure 11 and Table 5), and

oxidation of carbon can take place using the oxygen from the metal oxide (Fe_2O_3) in the vicinity of MgO.

MgO can easily be prepared using naturally occurring dolomite, and Fe_2O_3 can be obtained as naturally occurring mineral hematite, limonite, magnetite, and taconite. We have also demonstrated that it is possible to use a naturally occurring low-cost dolomite/hematite mixture as a potential oxygen carrier.

This study has revealed that the redox mechanism of MgO and Fe_2O_3 may provide an important link in enhancing the combustion of CH_4 for a CLC reaction. The material contact was more significant when the materials were prepared by a liquid impregnation method as compared to a solid mixing method. This may be a reason for carriers prepared with $Mg(OH)_2$ to perform better than those prepared with dolomite. The key feature of MgO is to improve the reactivity of the natural ore hematite as a promoter and not necessarily act as a support material to increase the surface area. Promotion activity may be due to a combination of several effects, but the activation of methane to form reaction intermediates may be the main contributor.

5.0 Conclusions

TGA, lab-scale flow-reactor data, and bench-scale flow-reactor data indicated that the addition of 5% MgO to the hematite oxygen carrier significantly improved the oxygen transfer capacity of hematite for methane CLC and correspondingly increased the amount of CO_2 produced, as compared to the pure hematite oxygen carrier. The addition of MgO via different sources (hydroxide, dolomite, and nitrate) resulted in different oxidation efficiencies of hematite. The MgO prepared by the impregnation route using $Mg(OH)_2$ resulted in the most significant improvement in the oxygen transfer capacity of the hematite carrier. The carrier prepared for fluidized-bed tests had a high attrition resistance. Both oxygen utilization and attrition resistance

remained stable during multi-cycle fluidized-bed tests. The surface area changes were minimal and XRD data also indicated minimal phase changes upon addition of MgO, indicating that the promotion is due to a chemical effect. The addition of MgO enhanced the rates of reduction of Fe_2O_3 significantly and was consistent with the improvement in the amount of oxygen used for reaction. The product analysis during the flow reactor data indicated that MgO promotes a CH_4 decomposition reaction to form carbon and hydrogen. When Fe_2O_3 is present in the vicinity of the MgO, the carbon may be readily oxidized and converted to CO_2, while H_2 is converted to H_2O.

ACKNOWLEDGMENT

We would like to thank Thomas Simonyi, Richard Eddy, and William Batton for their help and expertise in conducting the experiments on the hematite based oxygen carriers. This technical work was performed in support of the National Energy and Technology Laboratory's ongoing research in CO_2 capture in the Separations and Fuels Processing Division. Project number DE-FE0004000.

This project was funded by the Department of Energy, National Energy Technology Laboratory, an agency of the United States Government, through a support contract with URS Energy & Construction, Inc. Neither the United States Government nor any agency thereof, nor any of their employees, nor URS Energy & Construction, Inc., nor any of their employees, makes any warranty, expressed or implied, or assumes any legal liability or responsibility for the accuracy, completeness, or usefulness of any information, apparatus, product, or process disclosed, or represents that its use would not infringe privately owned rights. Reference herein to any specific commercial product, process, or service by trade name, trademark, manufacturer, or otherwise, does not necessarily constitute or imply its endorsement, recommendation, or favoring by the United States Government or any agency thereof. The views and opinions of authors expressed herein do not necessarily state or reflect those of the United States Government or any agency thereof.

REFERENCES

[1] Gayán P, Pans MA, Ortiz M, Abad A, de Diego LF, García-Labiano F, et al. Testing of a highly reactive impregnated Fe2O3/Al2O3 oxygen carrier for a SR–CLC system in a continuous CLC unit. Fuel Processing Technology. 2012;96:37-47.

[2] Adanez J, Abad A, Garcia-Labiano F, Gayan P, de Diego LF. Progress in Chemical-Looping Combustion and Reforming technologies. Progress in Energy and Combustion Science. 2012;38:215-82.

[3] Ksepko E, Sciazko M, Babinski P. Studies on the redox reaction kinetics of Fe2O3–CuO/Al2O3 and Fe2O3/TiO2 oxygen carriers. Applied Energy. 2014;115:374-83.

[4] Mayer F, Bidwe AR, Schopf A, Taheri K, Zieba M, Scheffknecht G. Comparison of a new micaceous iron oxide and ilmenite as oxygen carrier for Chemical looping combustion with respect to syngas conversion. Applied Energy. 2014;113:1863-8.

[5] Schwebel GL, Filippou D, Hudon G, Tworkowski M, Gipperich A, Krumm W. Experimental comparison of two different ilmenites in fluidized bed and fixed bed chemical-looping combustion. Applied Energy. 2014;113:1902-8.

[6] Tong A, Bayham S, Kathe MV, Zeng L, Luo S, Fan L-S. Iron-based syngas chemical looping process and coal-direct chemical looping process development at Ohio State University. Applied Energy. 2014;113:1836-45.

[7] Ku Y, Wu H-C, Chiu P-C, Tseng Y-H, Kuo Y-L. Methane combustion by moving bed fuel reactor with Fe2O3/Al2O3 oxygen carriers. Applied Energy. 2014;113:1909-15.

[8] Adánez-Rubio I, Arjmand M, Leion H, Gayán P, Abad A, Mattisson T, et al. Investigation of Combined Supports for Cu-Based Oxygen Carriers for Chemical-Looping with Oxygen Uncoupling (CLOU). Energy & Fuels. 2013;27:3918-27.

[9] Zhang Y, Liu F, Chen L, Han C, Richburg LR, Neathery JK, et al. Investigation of the Water Vapor Influence on the Performance of Iron-, Copper-, and Nickel-Based Oxygen Carriers for Chemical Looping Combustion. Energy & Fuels. 2013;27:5341-51.

[10] Sahir AH, Lighty JS, Sohn HY. Kinetics of Copper Oxidation in the Air Reactor of a Chemical Looping Combustion System using the Law of Additive Reaction Times. Industrial & Engineering Chemistry Research. 2011;50:13330-9.

[11] Wang S, Wang G, Jiang F, Luo M, Li H. Chemical looping combustion of coke oven gas by using Fe2O3/CuO with MgAl2O4 as oxygen carrier. Energy & Environmental Science. 2010;3.

[12] Lind F, Berguerand N, Seemann M, Thunman H. Ilmenite and Nickel as Catalysts for Upgrading of Raw Gas Derived from Biomass Gasification. Energy & Fuels. 2013;27:997-1007.

[13] Liu L, Zachariah MR. Enhanced Performance of Alkali Metal Doped Fe2O3 and Fe2O3/Al2O3 Composites As Oxygen Carrier Material in Chemical Looping Combustion. Energy & Fuels. 2013;27:4977-83.

[14] Bayham SC, Kim HR, Wang D, Tong A, Zeng L, McGiveron O, et al. Iron-Based Coal Direct Chemical Looping Combustion Process: 200-h Continuous Operation of a 25-kWth Subpilot Unit. Energy & Fuels. 2013;27:1347-56.

[15] Abad A, Adánez J, García-Labiano F, de Diego LF, Gayán P, Celaya J. Mapping of the range of operational conditions for Cu-, Fe-, and Ni-based oxygen carriers in chemical-looping combustion. Chemical Engineering Science. 2007;62:533-49.

[16] Abad A, García-Labiano F, de Diego LF, Gayán P, Adánez J. Reduction Kinetics of Cu-, Ni-, and Fe-Based Oxygen Carriers Using Syngas (CO + H2) for Chemical-Looping Combustion. Energy & Fuels. 2007;21:1843-53.

[17] Bhavsar S, Veser G. Reducible Supports for Ni-based Oxygen Carriers in Chemical Looping Combustion. Energy & Fuels. 2013;27:2073-84.

[18] Rydén M, Lyngfelt A, Mattisson T. Chemical-Looping Combustion and Chemical-Looping Reforming in a Circulating Fluidized-Bed Reactor Using Ni-Based Oxygen Carriers. Energy & Fuels. 2008;22:2585-97.

[19] Zafar Q, Abad A, Mattisson T, Gevert B. Reaction Kinetics of Freeze-Granulated NiO/MgAl2O4 Oxygen Carrier Particles for Chemical-Looping Combustion. Energy & Fuels. 2007;21:610-8.

[20] Abbasi M, Farniaei M, Rahimpour MR, Shariati A. Enhancement of Hydrogen Production and Carbon Dioxide Capturing in a Novel Methane Steam Reformer Coupled with Chemical Looping Combustion and Assisted by Hydrogen Perm-Selective Membranes. Energy & Fuels. 2013;27:5359-72.

[21] Hallberg P, Jing D, Rydén M, Mattisson T, Lyngfelt A. Chemical Looping Combustion and Chemical Looping with Oxygen Uncoupling Experiments in a Batch Reactor Using Spray-Dried CaMn1−xMxO3−δ (M = Ti, Fe, Mg) Particles as Oxygen Carriers. Energy & Fuels. 2013;27:1473-81.

[22] Zafar Q, Mattisson T, Gevert B. Integrated Hydrogen and Power Production with CO2 Capture Using Chemical-Looping ReformingRedox Reactivity of Particles of CuO, Mn2O3, NiO, and Fe2O3 Using SiO2 as a Support. Industrial & Engineering Chemistry Research. 2005;44:3485-96.

[23] Zafar Q, Mattisson T, Gevert B. Redox Investigation of Some Oxides of Transition-State Metals Ni, Cu, Fe, and Mn Supported on SiO2 and MgAl2O4. Energy & Fuels. 2005;20:34-44.

[24] Mattisson T, Järdnäs A, Lyngfelt A. Reactivity of Some Metal Oxides Supported on Alumina with Alternating Methane and OxygenApplication for Chemical-Looping Combustion. Energy & Fuels. 2003;17:643-51.

[25] Hedayati A, Azad A-M, Rydén M, Leion H, Mattisson T. Evaluation of Novel Ceria-Supported Metal Oxides As Oxygen Carriers for Chemical-Looping Combustion. Industrial & Engineering Chemistry Research. 2012;51:12796-806.

[26] Kidambi PR, Cleeton JPE, Scott SA, Dennis JS, Bohn CD. Interaction of Iron Oxide with Alumina in a Composite Oxygen Carrier during the Production of Hydrogen by Chemical Looping. Energy & Fuels. 2011;26:603-17.

[27] Adánez-Rubio I, Gayán P, Abad A, de Diego LF, García-Labiano F, Adánez J. Evaluation of a Spray-Dried CuO/MgAl2O4 Oxygen Carrier for the Chemical Looping with Oxygen Uncoupling Process. Energy & Fuels. 2012;26:3069-81.

[28] Johansson E, Mattisson T, Lyngfelt A, Thunman H. Combustion of Syngas and Natural Gas in a 300 W Chemical-Looping Combustor. Chemical Engineering Research and Design. 2006;84:819-27.

[29] Johansson E, Mattisson T, Lyngfelt A, Thunman H. A 300W laboratory reactor system for chemical-looping combustion with particle circulation. Fuel. 2006;85:1428-38.

[30] Song H, Doroodchi E, Moghtaderi B. Redox Characteristics of Fe–Ni/SiO2 Bimetallic Oxygen Carriers in CO under Conditions Pertinent to Chemical Looping Combustion. Energy & Fuels. 2011;26:75-84.

[31] Mattisson T, Johansson M, Lyngfelt A. The use of NiO as an oxygen carrier in chemical-looping combustion. Fuel. 2006;85:736-47.

[32] Ryden M, Johansson M, Lyngfelt A, Mattisson T. NiO supported on Mg-ZrO2 as oxygen carrier for chemical-looping combustion and chemical-looping reforming. Energy & Environmental Science. 2009;2.

[33] Son SR, Kim SD. Chemical-Looping Combustion with NiO and Fe2O3 in a Thermobalance and Circulating Fluidized Bed Reactor with Double Loops. Industrial & Engineering Chemistry Research. 2006;45:2689-96.

[34] Ryu H-J, Bae D-H, Han K-H, Lee S-Y, Jin G-T, Choi J-H. Oxidation and reduction characteristics of oxygen carrier particles and reaction kinetics by unreacted core model. Korean Journal of Chemical Engineering. 2001;18:831-7.

[35] Sim CY, Brown T, Chen Q, Sharifi V, Swithenbank J, Dennis J, et al. Particle characterisation in chemical looping combustion. Chemical Engineering Science. 2012;69:211-24.

[36] Zhu X, Wang H, Wei Y, Li K, Cheng X. Hydrogen and syngas production from two-step steam reforming of methane using CeO2 as oxygen carrier. Journal of Natural Gas Chemistry. 2011;20:281-6.

[37] Thon A, Kramp M, Hartge E-U, Heinrich S, Werther J. Operational experience with a system of coupled fluidized beds for chemical looping combustion of solid fuels using ilmenite as oxygen carrier. Applied Energy. 2014;118:309-17.

[38] Cao Y, Sit SP, Pan W-P. The development of 10-KW Chemical Looping Combustion Technology in ICSET, WKU. 2nd International Conference on Chemical Looping. Darmstadt, Germany2012.

[39] Linderholm C, Lyngfelt A, Dueso C. Chemical-looping combustion of solid fuels in a 10 kW reactor system using natural minerals as oxygen carrier. Energy Procedia. 2013;37:598-607.

[40] Mattisson T, Johansson M, Lyngfelt A. Multicycle reduction and oxidation of different types of iron oxide particles - Application to chemical-looping combustion. Energy & Fuels. 2004;18:628-37.

[41] Johansson M, Mattisson T, Lyngfelt A. Investigation of Fe2O3 with MgAl2O4 for Chemical-Looping Combustion. Industrial & Engineering Chemistry Research. 2004;43:6978-87.

[42] Ryden M, Cleverstam E, Johansson M, Lyngfelt A, Mattisson T. Fe2O3 on Ce-, Ca-, or Mg-Stabilized ZrO2 as Oxygen Carrier for Chemical-Looping Combustion Using NiO as Additive. AIChE Journal. 2010;56:2211-20.

[43] Ryden M, Johansson M, Cleverstam E, Lyngfelt A, Mattisson T. Ilmenite with addition of NiO as oxygen carrier for chemical-looping combustion. Fuel. 2010;89:3523-33.

[44] Jerndal E, Mattisson T, Thijs I, Snijkers F, Lyngfelt A. NiO particles with Ca and Mg based additives produced by spray- drying as oxygen carriers for chemical-looping combustion. Energy Procedia. 2009;1:479-86.

[45] Miller DD, Siriwardane R. Mechanism of Methane Chemical Looping Combustion with Hematite Promoted with CeO2. Energy & Fuels. 2013;27:4087-96.

[46] Baek JI, Kim JW, Lee JB, Eom TH, Ryu J, Ryu CK, et al. Effects of support on the performance of NiO-based oxygen carriers. Oil Gas Sci Technol. 2011;66:223-34.

[47] Qin C, Yin J, Liu W, An H, Feng B. Behavior of CaO/CuO Based Composite in a Combined Calcium and Copper Chemical Looping Process. Industrial & Engineering Chemistry Research. 2012;51:12274-81.

[48] Siriwardane R, Miller D. Regenerable MgO Promoted Metal Oxide Oxygen Carriers, S-130,411. 2012. p. 30.

[49] Ge X, Li M, Shen J. The Reduction of Mg–Fe–O and Mg–Fe–Al–O Complex Oxides Studied by Temperature-Programmed Reduction Combined with in Situ Mössbauer Spectroscopy. Journal of Solid State Chemistry. 2001;161:38-44.

[50] Siriwardane R, Tian H, Simonyi T, Poston J. Synergetic effects of mixed copper–iron oxides oxygen carriers in chemical looping combustion. Fuel. 2013;108:319-33.

[51] Abad A, Mattisson T, Lyngfelt A, Johansson M. The use of iron oxide as oxygen carrier in a chemical-looping reactor. Fuel. 2007;86:1021-35.

[52] Johansson M, Mattisson T, Lyngfelt A, Abad A. Using continuous and pulse experiments to compare two promising nickel-based oxygen carriers for use in chemical-looping technologies. Fuel. 2008;87:988-1001.

[53] Dueso C, Abad A, García-Labiano F, de Diego LF, Gayán P, Adánez J, et al. Reactivity of a NiO/Al2O3 oxygen carrier prepared by impregnation for chemical-looping combustion. Fuel. 2010;89:3399-409.

[54] Abad A, Mattisson T, Lyngfelt A, Johansson M. The use of iron oxide as oxygen carrier in a chemical-looping reactor. Fuel. 2007;86:1021-35.

[55] Monazam ER, Breault RW, Siriwardane R, Miller DD. Thermogravimetric Analysis of Modified Hematite by Methane (CH4) for Chemical-Looping Combustion: A Global Kinetics Mechanism. Industrial & Engineering Chemistry Research. 2013;52:14808-16.

[56] Li FX, Sun ZC, Luo SW, Fan LS. Ionic diffusion in the oxidation of iron-effect of support and its implications to chemical looping applications. Energy & Environmental Science. 2011;4:876-80.

[57] Konieczny A, Mondal K, Wiltowski T, Dydo P. Catalyst development for thermocatalytic decomposition of methane to hydrogen. International Journal of Hydrogen Energy. 2008;33:264-72.

[58] Ashok J, Raju G, Reddy PS, Subrahmanyam M, Venugopal A. Catalytic decomposition of CH4 over Ni-Al2O3-SiO2 catalysts: Influence of pretreatment conditions for the production of H2. Journal of Natural Gas Chemistry. 2008;17:113-9.

[59] Pinilla JL, Suelves I, Lázaro MJ, Moliner R, Palacios JM. Activity of NiCuAl catalyst in methane decomposition studied using a thermobalance and the structural changes in the Ni and the deposited carbon. International Journal of Hydrogen Energy. 2008;33:2515-24.

[60] Cunha AF, Órfão JJM, Figueiredo JL. Catalytic decomposition of methane on Raney-type catalysts. Applied Catalysis A: General. 2008;348:103-12.

[61] Echegoyen Y, Suelves I, Lázaro MJ, Moliner R, Palacios JM. Hydrogen production by thermocatalytic decomposition of methane over Ni-Al and Ni-Cu-Al catalysts: Effect of calcination temperature. Journal of Power Sources. 2007;169:150-7.

[62] Villacampa JI, Royo C, Romeo E, Montoya JA, Del Angel P, Monzón A. Catalytic decomposition of methane over Ni-Al2O3 coprecipitated catalysts: Reaction and regeneration studies. Applied Catalysis A: General. 2003;252:363-83.

[63] Venugopal A, Naveen Kumar S, Ashok J, Hari Prasad D, Durga Kumari V, Prasad KBS, et al. Hydrogen production by catalytic decomposition of methane over. International Journal of Hydrogen Energy. 2007;32:1782-8.

[64] Gac W, Denis A, Borowiecki T, Kepinski L. Methane decomposition over Ni-MgO-Al2O3 catalysts. Appl Catal, A. 2009;357:236-43.